iScience

CellPress
OPEN ACCESS

Article

Dual inhibition of aminoacyl-tRNA synthetase interacting multifunctional protein-2 and α-synuclein by steroid derivative is neuroprotective in Parkinson's model

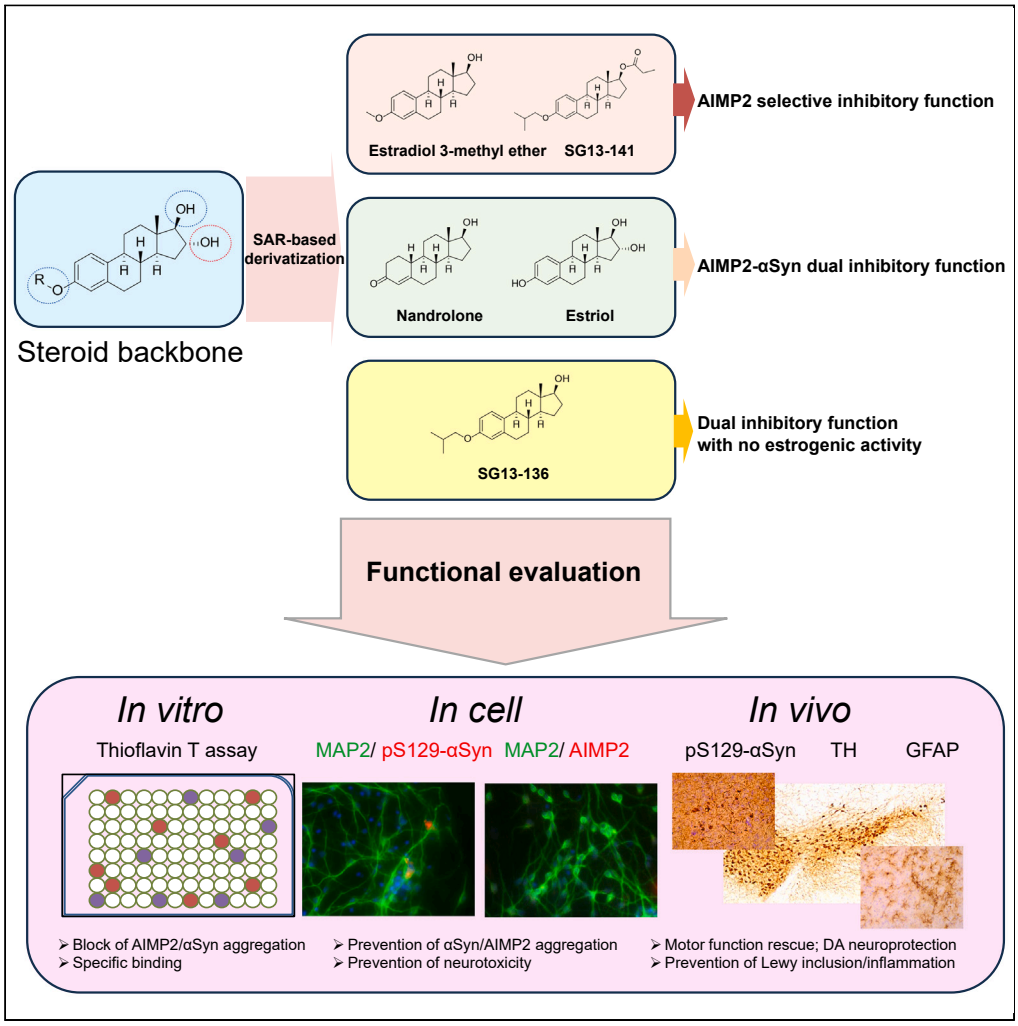

Jeong-Yong Shin, Min Woo Ha, Ji Hun Kim, Jiwon Cheon, Gum Hwa Lee, Seung-Mann Paek, Yunjong Lee

million@gnu.ac.kr (S.-M.P.)
ylee69@skku.edu (Y.L.)

Highlights

SAR-based synthesis of steroid derivatives targeting AIMP2 and α-synuclein inhibition

Estriol derivative SG13-136 binds AIMP2 and α-synuclein, blocking their aggregation

SG13-136 has no estrogen-related toxicity *in vitro* and *in vivo*

SG13-136 prevents PD-related pathologies in cellular and animal models of sporadic PD

Shin et al., iScience *27*, 111165
November 15, 2024
https://doi.org/10.1016/j.isci.2024.111165

iScience

CellPress
OPEN ACCESS

Article

Dual inhibition of aminoacyl-tRNA synthetase interacting multifunctional protein-2 and α-synuclein by steroid derivative is neuroprotective in Parkinson's model

Jeong-Yong Shin,[1,5] Min Woo Ha,[2,5] Ji Hun Kim,[1] Jiwon Cheon,[1] Gum Hwa Lee,[3] Seung-Mann Paek,[4,*] and Yunjong Lee[1,6,*]

SUMMARY

Aminoacyl-tRNA synthetase interacting multifunctional protein-2 (AIMP2), a parkin substrate, possesses self-aggregating properties, potentiating α-synuclein aggregation and neurotoxicity in PD. Thus, targeting both α-synuclein and AIMP2 would present an effective treatment for PD pathologies. Herein, we developed small compounds with dual inhibitory activity against AIMP2 and α-synuclein. Structure–activity relationship (SAR) analysis on commercial and newly synthesized steroid derivatives revealed critical chemical moieties for biological AIMP2 and α-synuclein inhibitory function. Among others, the new compound SG13-136 exhibited strong binding affinity and inhibitory function for both AIMP2 and α-synuclein *in vitro*. Importantly, in contrast to estriol and other steroids, SG13-136 lacked estrogenic activity, showing no overt toxicity *in vivo*. Furthermore, SG13-136 demonstrated therapeutic protective effects against PD pathologies in cellular and mouse models of α-synucleinopathy. Our study confirms the strategic validity of targeting both AIMP2 and α-synuclein in PD treatment and offers SAR information that could be used for PD drug discovery.

INTRODUCTION

Parkinson's disease (PD) is characterized by the progressive loss of midbrain dopaminergic neurons, which contributes to its cardinal motor symptoms.[1] Although current PD therapeutics aim to enhance dopaminergic transmission and improve motor impairments, targeting the underlying pathologies is crucial for treating the disease. Consequently, significant efforts have been made to prevent or inhibit α-synuclein aggregation, as this aberrant process is responsible for neurodegeneration and inflammation in PD pathogenesis.[2] α-Synuclein aggregation can be induced by various pathological conditions, including α-synuclein mutations, multiplication of the α-synuclein gene, c-Abl-mediated α-synuclein phosphorylation, and interactions with other disease-associated proteins or metabolites.[3–7] Among various approaches, small compound inhibitors of disease protein aggregation hold promise, as they could not only inhibit the aggregation process but also disaggregate already existing preformed disease protein aggregates.[8–10]

Previously, we identified estriol as an inhibitor for AIMP2 and α-synuclein.[9,11] AIMP2 is a parkin substrate, which accumulates in the postmortem PD patient brains.[5,12] Importantly, AIMP2 also aggregates under PD pathological conditions, and these AIMP2 preformed aggregates serve as seeds for accelerated α-synuclein pathologies.[5] Thus, estriol demonstrated significant efficacy in preventing the aggregation of both AIMP2 and α-synuclein in primary cultured cortical neurons treated with α-synuclein preformed fibrils compared to other AIMP2 inhibitors.[9] Although estriol could be effective as a disease-modifying therapy for modulating the progression of α-synuclein and AIMP2 pathologies in PD, the estrogenic side effects associated with its chronic administration raise significant concerns in translational research.

In this study, we synthesized various analogs by modifying the sidechains of the steroid backbone structure to eliminate the estrogenic activity of estriol while retaining AIMP2 and α-synuclein inhibiting biological activity. Using a simple *in vitro* thioflavin T assay to monitor AIMP2 and α-synuclein recombinant protein aggregation, we identified structure–activity relationship of steroid derivatives revealing key elements for biological activity and selectivity of AIMP2, α-synuclein aggregation inhibition. Compound SG13-136 presented dual inhibitory functions against AIMP2 and α-synuclein without any estrogenic activity, resulting in therapeutic effects in neuronal and mouse models of

[1]Department of Pharmacology, Sungkyunkwan University School of Medicine, Samsung Biomedical Research Institute, Suwon 16419, Republic of Korea
[2]Jeju Research Institute of Pharmaceutical Sciences, College of Pharmacy, Jeju National University, 102 Jejudaehak-ro, Jeju 63243 Jeju-do, Republic of Korea
[3]College of Pharmacy, Chosun University, Gwangju 61452, Republic of Korea
[4]College of Pharmacy and Research Institute of Pharmaceutical Sciences, Gyeongsang National University, 501 Jinju-daero, Jinju 52828, Gyeongnam-do, Republic of Korea
[5]These authors contributed equally
[6]Lead contact
*Correspondence: million@gnu.ac.kr (S.-M.P.), ylee69@skku.edu (Y.L.)
https://doi.org/10.1016/j.isci.2024.111165

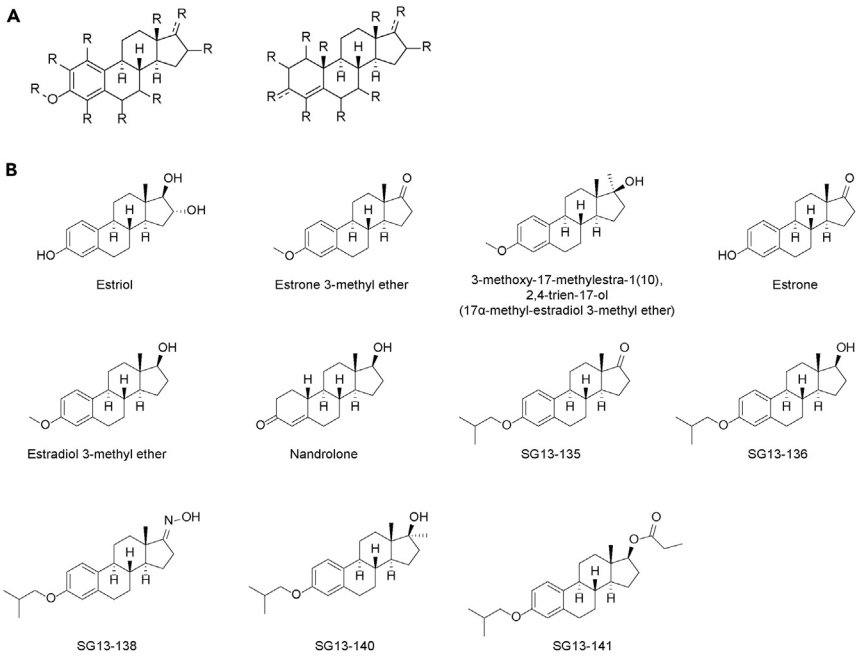

Figure 1. Chemical structure of steroid hormone analogs and derivatives synthesized for biological activity assessment for AIMP2 and α-synuclein aggregation inhibition

(A) Chemical backbone of steroid hormone. Modifications were made at the R positions to influence biological activity.

(B) Chemical structures of the steroid hormone derivatives. Synthesized compounds were named as SG13-135, SG13-136, SG13-138, SG13-140, and SG13-141.

α-synucleinopathy. Our study suggests that the dual inhibition of AIMP2 and α-synuclein aggregation could be an effective strategy for modifying the progression of PD.

RESULTS

Synthesis of steroid derivatives to improve biological activity inhibiting aminoacyl-tRNA synthetase interacting multifunctional protein-2 and α-synuclein

Previously, we showed that estriol possesses the biological activity to inhibit the aggregation of both α-synuclein and AIMP2 *in vitro*. To analyze the structure–activity relationship of commercially available compounds related to estriol, we procured several commercially available steroid derivatives, including estrone 3-methyl ether, 3-methoxy-17-methylestra-1(10),2,4-trien-17-ol, estrone, estradiol 3-methyl ether, and nandrolone (Figures 1A and 1B). Moreover, to develop new steroid derivatives with inhibitory activity against AIMP2 and α-synuclein, we synthesized compounds (Figure 1B and Data S1) by modifying the side chains of the A and D rings of the steroid backbone structure for subsequent biological activity assays.

To synthesize analogs, we introduced an isobutyl side chain to estrone. This bulky side chain was envisaged to differentiate its effect in inhibiting α-synuclein aggregation from its binding to estrogen receptor. Following a direct substitution reaction, hydride reduction was performed to produce the desired product SG13-136 in excellent yield (Figure 1B and Data S1). To assess and improve the biological activity of inhibiting AIMP2 and α-synuclein, other analogs were prepared through ketoxime introduction, or Grignard reaction, or Fischer esterification. Finally, a biotin-conjugated analog of the estrone skeleton was synthesized using Click chemistry (Figure 1B and Data S1).

Steroid derivatives with the inhibitory function of aminoacyl-tRNA synthetase interacting multifunctional protein-2 and α-synuclein aggregation *in vitro*

To compare the inhibitory effects of estriol and commercially available steroid derivatives, we conducted a thioflavin T assay to monitor the potential inhibition of the amyloid aggregation of recombinant AIMP2 and α-synuclein proteins *in vitro*. When recombinant AIMP2 was incubated for three days in a test tube, the relative thioflavin T fluorescence increased by about 4-fold, indicating amyloid aggregation of AIMP2 (Figure 2A). Consistent with previous reports,[9] estriol blocked this increase in thioflavin T fluorescence caused by AIMP2 aggregation (Figure 2A). Furthermore, both estradiol 3-methyl ether and nandrolone exhibited nearly complete inhibition of AIMP2 aggregation to an extent similar to estriol (Figure 2A). Estrone showed only modest inhibition of AIMP2 aggregation compared to estriol (Figure 2A). Additionally, we examined the biological activity against α-synuclein aggregation using a thioflavin T assay with recombinant α-synuclein incubated in a test tube. Estriol largely blocked the approximate 3-fold increase in thioflavin T fluorescence resulting from a three-day incubation of recombinant

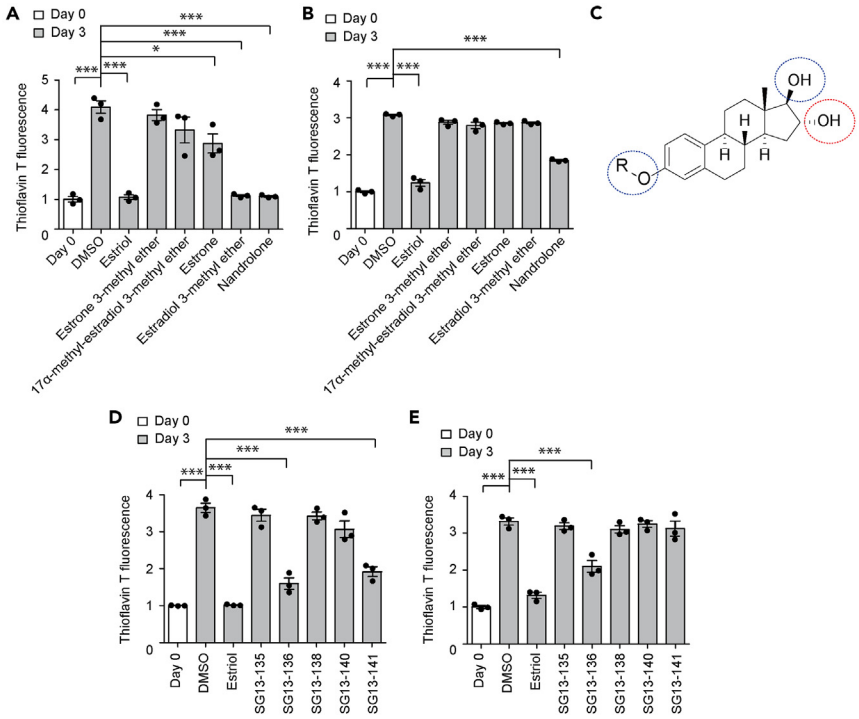

Figure 2. Development of steroid derivatives with selective biological inhibitory activity against AIMP2 or α-synuclein aggregation

(A) Amyloid-like aggregation of recombinant AIMP2 incubated for three days (1 μM in PBS) in the presence of indicated compounds (50 μM), monitored by thioflavin T fluorescence assay (n = 3 per group). Thioflavin T measurement of recombinant AIMP2 at day 0 served as a baseline, with DMSO as vehicle control.

(B) Amyloid-like aggregation of recombinant α-synuclein incubated for 3 days (1 μM in PBS) in the presence of the indicated compounds (50 μM), monitored by thioflavin T fluorescence assay (n = 3 per group). Thioflavin T measurement of recombinant α-synuclein at day 0 served as baseline, with DMSO as vehicle control.

(C) Relationship between chemical structure and biophysical activity of steroid derivatives inhibiting AIMP2 and/or α-synuclein aggregation *in vitro*. Residues associated with AIMP2 and α-synuclein aggregation inhibition were circled with blue and red dotted circles, respectively.

(D) Amyloid-like aggregation of recombinant AIMP2 incubated for three days (1 μM in PBS) in the presence of synthesized compounds (50 μM), monitored by thioflavin T fluorescence assay (n = 3 per group). Thioflavin T measurement of recombinant AIMP2 at day 0 served as a baseline, with DMSO as vehicle control. Estriol was used as a reference positive control.

(E) Amyloid-like aggregation of recombinant α-synuclein incubated for three days (1 μM in PBS) in the presence of the synthesized compounds (50 μM), monitored by thioflavin T fluorescence assay (n = 3 per group). Thioflavin T measurement of recombinant α-synuclein at day 0 served as baseline, with DMSO as vehicle control. Estriol was used as a reference positive control. Data in all panels represent mean ± standard error of the mean. *$p < 0.05$ and ***$p < 0.001$, determined by two-way analysis of variance (ANOVA) followed by Tukey's post hoc analysis.

α-synuclein protein, and most of the other steroid derivatives failed to inhibit α-synuclein aggregation, except for nandrolone, which showed about 39.9% inhibition of α-synuclein aggregation (Figure 2B).

Considering that the side chain in the A ring and the -OH groups in the D ring of the steroid backbone are linked to inhibitory functions for AIMP2 and α-synuclein aggregation (Figure 2C), we further investigated the potential modulation of AIMP2 and α-synuclein aggregation by steroid derivatives synthesized through alterations of these side chains. The compound SG13-136, which features a simple secondary alcohol group in the D ring and an isobutyl ether moiety in the A ring, showed the inhibition of both AIMP2 and α-synuclein aggregation in a thioflavin T assay (Figures 2D and 2E). While the degree of inhibitory activity of SG13-136 for AIMP2 and α-synuclein was slightly reduced compared to estriol, SG13-136 still provided 56.2% and 36.7% inhibition of AIMP2 and α-synuclein aggregation, respectively (Figures 2D and 2E). Conversely, SG13-141, which has a propionyl ester functionality on the D ring, showed selective AIMP2 aggregation inhibition without affecting α-synuclein aggregation (Figures 2D and 2E). In summary, we investigated structure–activity relationship using a repertoire of commercially available steroid derivatives and newly synthesized compounds and identified important functional modalities that determine efficacy and selectivity for AIMP2 and α-synuclein aggregation inhibition (Table S1).

Steroid derivatives with the dual inhibition of aminoacyl-tRNA synthetase interacting multifunctional protein-2 and α-synuclein aggregation but no estrogenic activity

In *in vitro* thioflavin T aggregation assays, we identified new steroid derivatives (including estriol as a positive control, estradiol 3-methyl ether, nandrolone, SG13-138, and SG13-141) that possess inhibitory functions against AIMP2 aggregation. We aimed to determine whether these AIMP2-inhibiting compounds exhibit cytoprotective effects against AIMP2 toxicity in cells. SH-SY5Y neuroblastoma cells were transfected

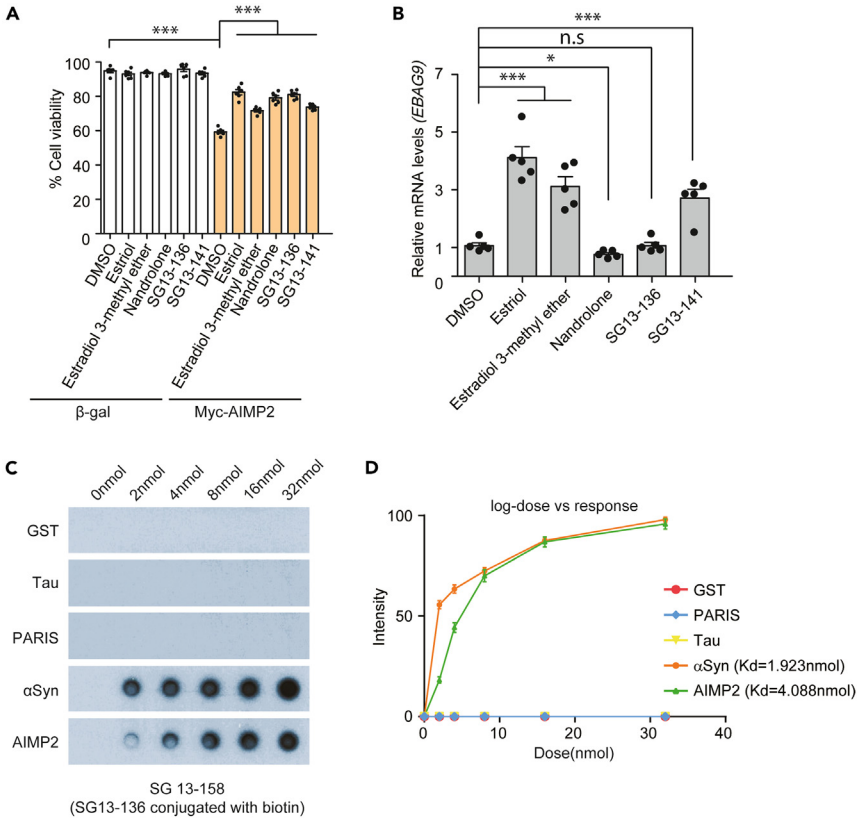

Figure 3. Compound displaying dual inhibitory activity against AIMP2 and α-synuclein aggregation without estrogenic activity

(A) Trypan blue exclusion cell viability assessment conducted in SH-SY5Y cells transfected with Myc-AIMP2 or β-gal control (72 h) and treated with indicated compounds for AIMP2 and/or α-synuclein inhibitory activity (10 μM, 48 h) (n = 6 per group).

(B) Quantification of estrogen responsive gene, *EBAG9* messenger RNA levels in the human breast tumor cell line, MCF7 treated with the indicated compounds (10 μM, 48 h) (n = 5 separate experiments per group). *GAPDH* served as internal loading control for normalization.

(C) Dot blot assessment of biotin-conjugated SG13-136 (SG13-158: 0, 2, 4, 8, 16, and 32 nmol) binding to recombinant α-synuclein (αSyn) or/and AIMP2 (1 μg). SG13-136 binding to recombinant GST, Tau, and ZNF746 (1 μg) was also monitored to determine the specificity of SG13-136 binding to α-synuclein and AIMP2.

(D) Binding curve depicting increasing doses of biotin-conjugated SG13-136 for each recombinant protein in the dot blot assay. Dissociation constant (K_d) values of biotin-conjugated SG13-136 binding to α-synuclein and AIMP2 are provided. Data in all panels represent mean ± standard error of the mean. *$p < 0.05$ and ***$p < 0.001$, determined by one-way (B) or two-way (A) analysis of variance (ANOVA) followed by Tukey's post hoc analysis. n.s., non-significant.

with Myc-AIMP2, resulting in approximately 40.7% cytotoxicity (Figure 3A). In contrast, β-gal overexpression control had no cytotoxicity with comparable cell viability to that of Myc empty plasmid transfection (Figure S1A). Thus, in the subsequent cell viability analysis β-gal was used as a control for Myc-AIMP2 overexpression. Consistent with the previous report,[9] estriol, an AIMP2 inhibitor, largely prevented AIMP2-induced cell death (Figure 3A). Other AIMP2 inhibitors also showed varying degrees of cytoprotection against AIMP2 overexpression in SH-SY5Y cells. Among these steroid derivatives, apart from estriol, the most effective protection against AIMP2-induced cytotoxicity in SH-SY5Y cells was observed with nandrolone and SG13-136 (Figure 3A), both of which showed the dual inhibition of AIMP2 and α-synuclein aggregation *in vitro* (Figure 2). None of the steroid derivatives tested at 10 μM showed any obvious toxicity in β-gal transfected control SH-SY5Y cells (Figure 3A).

Next, we evaluated the estrogenic activity of these steroid derivatives. Estrogen receptor binding by ligand in MCF7 cells induces the transcription of target genes such as *EBAG9* and *CCND1*.[13] As expected, estriol and estradiol 3-methyl ether, which have shown estrogenic activity previously, increased the transcript levels of *EBAG9* and *CCND1* in MCF7 cells (Figures 3B and S1B). Nandrolone, developed as an androgen receptor agonist,[14] suppressed the expression of *EBAG9* and *CCND1* mRNAs (Figures 3B and S1B). SG13-141 showed estrogen receptor activation to a similar extent as estradiol 3-methyl ether (Figures 3B and S1B). SG13-136 showed no alteration in both *EBAG9* and *CCND1* transcription (Table S1). Moreover, the expression of additional estrogen target genes (*E2F1*, and *BCL2*) was not altered by SG13-136 treatment in MCF7 cells (Figures S1C and S1D), indicating no binding to the estrogen receptor and modulation by SG13-136. Since SG13-136 showed no estrogenic activity, we compared its potential cytotoxicity in SH-SY5Y cells using a trypan blue exclusion assay. While estriol treatment resulted in approximately 50% cell viability at 200 μM and further reduced cell viability to ~30% at 500 μM, SG13-136 led to saturated cell viability of ~56% at high doses of 200 and 500 μM in SH-SY5Y cells (Figure S1E).

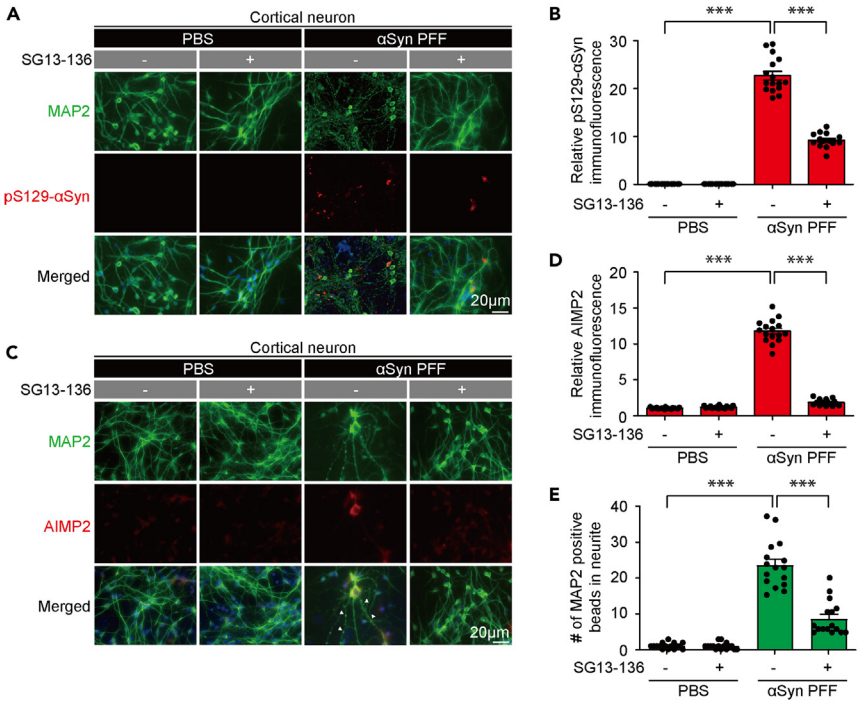

Figure 4. Steroid derivative, SG13-136, prevents αSyn PFF-induced aggregation of α-synuclein and AIMP2 in cortical neurons

(A) Representative co-immunofluorescence images depict the expression and distribution of pS129-αSyn in MAP2-labeled primary cultured cortical neurons treated with α-synuclein preformed fibril (αSyn PFF, 1 μg/mL, 10 days) in the presence or absence of SG13-136 (10 μM, 8 days). Scale bar = 20 μm.

(B) Quantification of relative immunofluorescence signals of pS129-αSyn in the indicated experimental groups (n = 16 fluorescence images from three separate experiments per group).

(C) Representative co-immunofluorescence images illustrate the expression and distribution of AIMP2 in MAP2-labeled primary cultured cortical neurons treated with α-synuclein preformed fibril (αSyn PFF, 1 μg/mL, 10 days) in the presence or absence of SG13-136 (10 μM, 8 days). Scale bar = 20 μm.

(D) Quantification of relative immunofluorescence signals of AIMP2 in the indicated experimental groups (n = 16 fluorescence images from three separate experiments per group).

(E) Assessment of neural toxicity quantified as fragment counts of MAP2-positive neurites in each experimental group (n = 16 fluorescence images from three separate experiments per group). Data in all panels represent mean ± standard error of the mean. ***$p < 0.001$, determined by two-way ANOVA test followed by Tukey's post hoc analysis.

We investigated the mechanistic specificity of SG13-136 for inhibiting AIMP2 and α-synuclein by examining the direct physical interaction between the compound and recombinant proteins. Thus, we synthesized biotin-conjugated SG13-136 (named SG13-158) by adding a biotin tag to the side chain of the A ring (Figure S1F). The binding of biotinylated SG13-136 to recombinant α-synuclein, AIMP2, and unrelated protein controls were determined using a dot blot assay, applying increasing concentrations of biotin-conjugated SG13-136. SG13-136 specifically binds to α-synuclein and AIMP2, with no binding observed to GST, Tau, and PARIS (Figures 3C and 3D). Binding plots for SG13-136 with α-synuclein and AIMP2 showed saturating curves, with approximately 2-fold higher affinity for α-synuclein (Kd = 1.923 nmol) compared to AIMP2 (Kd = 4.088 nmol) (Figure 3D). Consistent with this specific binding profile of SG13-136 and no binding to Tau, Tau aggregation *in vitro* was not affected by SG13-136 as assessed by thioflavin T assay (Figure S1G). These results collectively suggest that the selective and specific binding of SG13-136 may contribute to AIMP2 aggregation inhibition *in vitro* and in cells, providing cytoprotection against AIMP2 overexpression in SH-SY5Y cells and exhibiting no estrogenic effects in MCF7 cells.

SG13-136 prevents α-synuclein and AIMP2 aggregation induced by α-synuclein preformed fibril in primary cortical neurons

SG13-136 showed dual inhibitory effects against both AIMP2 and α-synuclein aggregation. Therefore, we sought to determine whether SG13-136 could prevent neurotoxicity in a Parkinson's disease cell model, which has exhibited neurotoxicity due to both AIMP2 and α-synuclein aggregation.[5,9] The treatment of primary cultured cortical neurons with α-synuclein preformed fibril (αSyn PFF) induced robust α-synuclein aggregation, as evidenced by an increase in pS129-αSyn signals, along with AIMP2 aggregation (Figures 4A–4D). Consistent with our *in vitro* results demonstrating dual inhibitory activity against AIMP2 and α-synuclein aggregation, SG13-136 treatment to αSyn PFF treated cortical neurons prevented the induction of both α-synuclein and AIMP2 aggregation (Figures 4A–4D). Although SG13-136 partially blocked α-synuclein aggregation seeded by αSyn PFF in neurons, its treatment almost completely halted neuronal AIMP2

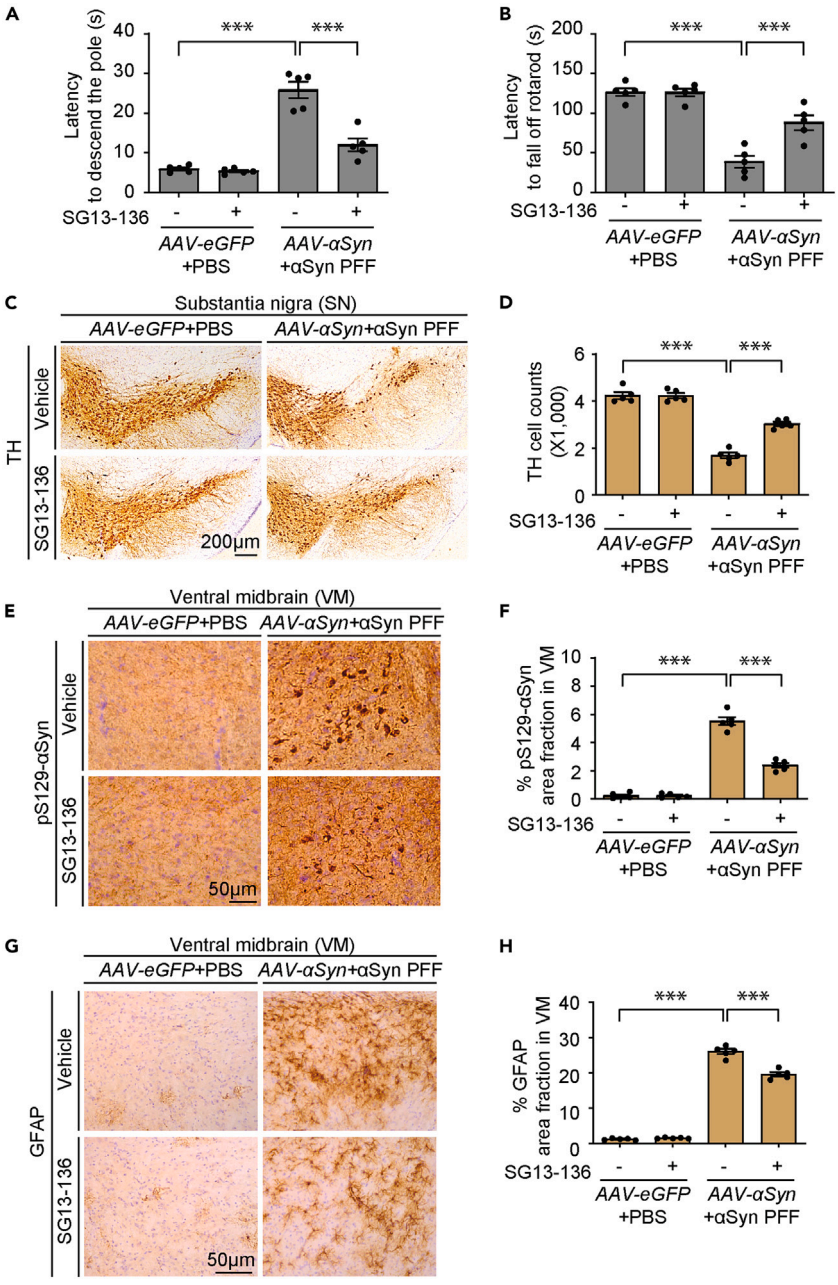

Figure 5. Steroid derivative, SG13-136, alleviates PD pathologies in a mouse model of αSyn PFF injection

(A) Assessment of bradykinesia in mice with nigral AAV-αSyn/αSyn PFF (10 μg) or AAV-eGFP/PBS injection as a control, administered SG13-136 (0.5 mg/kg, p.o. once daily for three weeks), or vehicle, monitored by pole test (n = 5 mice per group).

(B) Assessment of motor coordination in mice with nigral AAV-αSyn/αSyn PFF (10 μg) or AAV-eGFP/PBS injection as a control, administered SG13-136 (0.5 mg/kg, p.o. once daily for three weeks), or vehicle, monitored by rotarod test (n = 5 mice per group).

(C) Representative anti-TH immunohistochemistry images of ventral midbrain dopaminergic neurons from each mouse group with indicated nigral injections and SG13–136 p.o. administration. Scale bar = 200 μm.

(D) Stereological counting of TH-stained dopaminergic neurons in the substantia nigra pars compacta of the indicated experimental groups (n = 5 mice per group).

(E) Representative immunohistochemistry images displaying pS129-αSyn positive Lewy-like inclusions in ventral midbrain sections from mice with nigral AAV-αSyn/αSyn PFF (10 μg) or AAV-eGFP/PBS injection as a control, administered SG13-136 (0.5 mg/kg, p.o. once daily for three weeks), or vehicle. Scale bar = 50 μm.

(F) Quantification of % area fraction with pS129-αSyn staining in the ventral midbrain sections from each mouse group (n = 5 mice per group).

Figure 5. *Continued*

(G) Representative anti-GFAP immunohistochemistry images demonstrating astrogliosis in ventral midbrain sections from mice with nigral AAV-αSyn/αSyn PFF (10 μg) or AAV-eGFP/PBS injection as a control, administered SG13-136 (0.5 mg/kg, p.o. once daily for three weeks), or vehicle. Scale bar = 50 μm.

(H) Quantification of % area fraction with GFAP staining in ventral midbrain sections from each mouse group (n = 5 mice per group). Data in all panels represents mean ± standard error of the mean. ***$p < 0.001$, determined by two-way analysis of variance (ANOVA) test followed by Tukey's post hoc analysis.

aggregation (Figures 4A–4D). Along with inhibiting AIMP2 and α-synuclein aggregation, SG13-136 treatment markedly prevented robust αSyn PFF-induced neurite beading, which serves as an indicator of neuronal toxicity in cortical neurons (Figure 4E).

Pathologies in a combinatorial α-synucleinopathy model of Parkinson's disease are alleviated by the administration of dual α-synuclein/aminoacyl-tRNA synthetase interacting multifunctional protein-2 inhibitor SG13-136

To assess and compare the safety profiles of SG13-136 and estriol *in vivo*, C57/BL6 male mice were orally administered daily for 21 days. Although SG13-136 and vehicle administration did not affect body weight gain in mice, estriol led to a reduction in body weight that was maintained throughout the administration period (Figure S2A). Moreover, after three weeks of estriol administration, the mice exhibited increased latency in the pole test and decreased latency in the rotarod test, indicating impaired motor function (Figures S2B and S2C). Conversely, mice administered SG13-136 exhibited motor performance similar to those receiving the vehicle (Figures S2B and S2C), indicating no adverse effects on motor function. The estrogenic effects of estriol and SG13-136 on the brain were also monitored using real-time quantitative PCR to measure estrogen target genes, *Ebag9* and *Ccnd1*. Estriol administration resulted in a significant increase in *Ebag9* and *Ccnd1* messenger RNA levels, while SG13-136 did not alter the transcription of these genes compared to the dimethyl sulfoxide vehicle control (Figures S2D and S2E). In addition, liver tissues from mice with SG13-136 oral administration showed similar expression levels of *Ebag9* and *Ccnd1* messenger RNAs as compared to those of dimethyl sulfoxide vehicle control (Figures S2F and S2G), further demonstrating no estrogenic activity of SG13-136. The potential *in vivo* toxicity of SG13-136 at the organ levels was examined by observing H&E stained sections from the heart, liver, kidney, lung, and spleen. No obvious abnormalities and alterations in gross structures were observed in tissues from mice administrated SG13-136 compared to those from vehicle-administered mice (Figure S2H).

Next, the therapeutic efficacy of SG13-136 in a mouse model of PD was determined. For this, we employed an α-synucleinopathy mouse model involving combinatorial injections of αSyn PFF and AAV-αSyn virus into the ventral tegmental area and substantia nigra, respectively. Coimmunofluorescence imaging revealed efficient transduction of ventral midbrain dopaminergic neurons by stereotaxic injections of either AAV-eGFP or AAV-αSyn (Figures S2I and S2J). Consistent with previous reports,[5,15] the combined injections of AAV-αSyn and αSyn PFF resulted in delayed performance in the pole test and reduced latency to stay on the accelerating rotarod, both indicative of motor function impairment (Figures 5A and 5B). Oral administration of SG13-136 notably prevented this motor function impairment in the combinatorial α-synucleinopathy mouse model (Figures 5A and 5B). SG13-136 administration did not affect motor functions in control mice injected with AAV-eGFP and PBS compared to those receiving the vehicle (Figures 5A and 5B), indicating no adverse effects on motor function in the control group. Consistent with the motor function impairment, the number of TH-positive dopaminergic neurons in the substantia nigra pars compacta was robustly reduced by 59.8% following nigral coinjections of AAV-αSyn and αSyn PFF. SG13-136 administration mitigated this nigral dopaminergic neurotoxicity by 28.4% (Figures 5C and 5D). No dopaminergic toxicity was observed when SG13-136 was administered to control mice injected with AAV-eGFP and PBS (Figures 5C and 5D). Reflecting the loss of dopaminergic neuron cell bodies in the substantia nigra, the α-synucleinopathy mouse model showed a substantial reduction in dopaminergic axon terminal densities in the striatum (Figure S2K and S2L). This degeneration of the dopaminergic axon terminal in the PD mouse model with combinatorial injections was largely prevented by 35% with SG13-136 administration (Figure S2K and S2L).

Neuronal α-synuclein aggregation can be induced by combinatorial injections of AAV-αSyn and αSyn PFF into the ventral midbrains.[5,15] Consistent with these reports, our combinatorial α-synucleinopathy PD mouse model developed strong pS129-αSyn immunoreactivity in the substantia nigra (Figures 5E and 5F), suggesting the formation of Lewy-like inclusions. Supporting the inhibitory activity of SG13-136 against α-synuclein aggregation observed *in vitro* and in cells, oral administration of SG13-136 substantially reduced the presence of pS129-αSyn positive Lewy-like inclusions in the midbrains of the PD model of α-synucleinopathy (Figures 5E and 5F). Along with dopaminergic neurodegeneration and α-synuclein aggregation, astrogliosis, assessed by anti-GFAP immunohistochemistry, was significantly increased in the midbrain sections of the mice receiving nigral AAV-αSyn and αSyn PFF injections (Figures 5E and 5F). This neuroinflammation was modestly decreased in the ventral midbrain sections from the PD mouse model that received SG13-136 administration (Figures 5G and 5H). Collectively, these *in vivo* studies demonstrate that SG13-136 can serve as a safe and effective disease-modifying drug, suppressing α-synuclein aggregation, dopaminergic neurodegeneration, and neuroinflammation, thus contributing to the improvement of motor impairment in the PD mouse model of α-synucleinopathy.

DISCUSSION

Herein, we introduced a screening assay platform and discovered disease-modifying small compounds with dual inhibitory functions targeting two PD-associated disease proteins—AIMP2 and α-synuclein. Both AIMP2 and α-synuclein have a tendency to misfold (with the transition of secondary structure from α-helix to β-strand), eventually forming amyloid-like aggregates *in vitro*.[5,16] Several studies have conducted screening for small compounds with biological activity to inhibit either α-synuclein or AIMP2 aggregation.[9,17] Thioflavin T fluorescence, which is sensitive to amyloid formation, can quantify the amount of amyloid formation of recombinant proteins during test-tube incubation. Previously, we successfully identified several AIMP2-inhibiting compounds using an *in vitro* AIMP2 aggregation monitoring platform based on

thioflavin T fluorescence.[9] Estriol, one of the estrogens, has been shown to inhibit both AIMP2 and α-synuclein aggregation.[9,11] In this study, we replicated the strong dual inhibitory function of estriol for both AIMP2 and α-synuclein *in vitro*. We utilized a library of synthesized and commercially available compounds with structures similar to estriol to measure and compare their inhibitory activity for AIMP2 and α-synuclein aggregation *in vitro* (Table S1). Through structure–activity relationship analysis, we identified that two hydroxyl groups on the D ring of estriol are crucial for its dual inhibitory function. Supporting this finding, compounds such as nandrolone, estradiol 3-methyl ether, and SG13-136, which have only one hydroxyl group on the D ring, showed diminished α-synuclein inhibiting activity while maintaining comparable AIMP2 inhibiting activity compared to estriol. Additionally, side chains on the A ring hydroxyl moiety of the steroid backbone also affected the efficacy of AIMP2 and/or α-synuclein aggregation inhibition. Compounds such as nandrolone with a carbonyl group in the six carbon A ring and SG13-136 with an isobutyl ether moiety in the A phenyl ring exhibited modest α-synuclein inhibiting activity, whereas estradiol 3-methyl ether with a methyl ether in the A phenyl ring failed to sustain α-synuclein inhibiting activity. All these compounds showed AIMP2 inhibiting functions. Pharmacological chaperones are small molecules with biological activity to enhance the stability of specific proteins, thus preventing their misfolding and aggregation.[18] In this regard, SG13-136 might function as a pharmacological chaperone of moderate-affinity to stabilize native structure of AIMP2 and α-synuclein. To support this notion, SG13-136 showed rather specific physical interaction with AIMP2, and α-synuclein (Kd, 40.88 μM, and 19.23 μM, respectively) without demonstrable binding to other disease-associated proteins such as PARIS, and tau (Figures 3C and 3D). Correlating with SG13-136's specific binding to AIMP2 and α-synuclein is the inhibition of their misfolding and amyloid-like aggregation (Figures 2D and 2E). Our SAR analysis could further help screen for more potent and safe inhibitors (pharmacological chaperone) for AIMP2 and/or α-synuclein aggregation in the future.

The steroid derivative SG13-136 directly binds to both recombinant AIMP2 and α-synuclein (Figures 3C and 3D). Although this binding inhibits the aggregation of AIMP2 and α-synuclein, it remains unclear whether SG13-136 can disaggregate preformed α-synuclein and AIMP2 fibrils. Estriol has previously been shown to disaggregate preformed AIMP2 and α-synuclein aggregates *in vitro*,[9,11] thus further investigation into the potential disaggregating activity of SG13-136 for preformed AIMP2 and α-synuclein *in vitro* would be informative. Compounds capable of reversing aggregation would be clinically advantageous for treating patients with advanced PD whose brains are already lesioned and affected by widespread preexisting AIMP2 and α-synuclein aggregate pathologies.

Steroid derivatives offer advantages in treating brain disorders due to their small size and lipid solubility, facilitating robust distribution in the brain.[19] Thus, estriol derivatives, including SG13-136, would probably possess favorable pharmacokinetic properties for application in neurodegenerative brain diseases. Estrogen receptor activation by estrogen and its derivatives leads to the transcription of diverse sets of genes depending on tissues, mediating different physiological functions. It should be noted that many studies have shown the dopaminergic neuroprotective function of estrogen in a toxin-induced PD mouse model.[20,21] Estrogen binding to its receptors in brains can activate the extracellular signal-regulated kinases and phosphoinositol-3-kinase-Akt signal transduction pathways that are potentially involved in neuroprotection.[22] However, the potential estrogenic activity of steroid derivatives raises potential concerns about potential adverse effects such as weight loss, hepatotoxicity, and an increased risk of stroke and breast cancer,[23–25] especially with high doses and long-term treatment. Indeed, estriol administration to male mice resulted in a reduction of body weight, while SG13-136, lacking estrogenic activity, had no effect on body weight. Although SG13-136 showed no overt toxicity in various organs at the tested dosage, liver toxicity was noted when a higher dose of SG13-136 was administered. Despite almost complete inhibition of α-synuclein aggregation and modest AIMP2 aggregation inhibition *in vitro*, the *in vivo* therapeutic effect of SG13-136 was relatively modest in the α-synucleinopathy mouse model (Figure 5). These data suggest that the dosage of SG13-136 *in vivo* was not sufficient to achieve maximal therapeutic efficacy. However, the toxicity of SG13-136 at high dosage *in vivo* hampered the evaluation of improved therapeutic efficacy with dosage elevation. It would be essential to develop more potent AIMP2 and α-synuclein dual inhibitors with no toxicity *in vivo*, allowing for the implementation of higher dosages to achieve maximal efficacy in inhibiting AIMP2 and α-synuclein. In addition, further *in vivo* studies using a larger cohort and both genders of mice would be needed to strengthen the conclusion of this study and expand its translational application.

Limitations of the study

As with any study reporting the biological functions of small compounds, the steroid derivatives identified here for the selective inhibition of AIMP2 or α-synuclein may interact with other proteins or macromolecules, potentially affecting signaling pathways beyond the AIMP2/α-synuclein aggregation process. However, we showed that SG13-136 selectively binds to α-synuclein and AIMP2, without interacting with GST, tau, or PARIS, and does not inhibit tau aggregation. To further assess potential nonspecific interactions, it would be valuable to evaluate a biotinylated version of SG13-136 in a 20,000-human-protein chip assay to predict other binding partners and potential side effects *in vivo*.

It is important to note that SG13-136's *in vivo* effects were evaluated in a single PD animal model involving AAV-αSyn/α-synuclein PFF combinatorial injections. While this model replicates key aspects of sporadic PD, it does not capture AIMP2 accumulation seen in certain PD subtypes. In cell models, SG13-136 demonstrated cytoprotective effects against AIMP2 overexpression in SH-SY5Y cells and neuroprotection in cortical neurons with α-synuclein PFF seeding. To confirm SG13-136's dual inhibitory function *in vivo*, further studies using alternative PD models that simulate AIMP2 accumulation, such as brain AAV-AIMP2 injections or combinatorial AAV-AIMP2/α-synuclein injections, are needed.

RESOURCE AVAILABILITY

Lead contact

Further information or requests for resources and reagents used in this study will be fulfilled by the Lead Contact, Yunjong Lee (ylee69@skku.edu).

Materials availability

Detailed procedures and structural validation for the synthesis of compounds are provided in the article. More information or request for these compounds can be directed to the lead contact, Yunjong Lee (ylee69@skku.edu).

Data and code availability

- Data: Imaging/fluorescence spectrometry data and mass spectrometry/IR analysis for the new compounds are provided in the article and further details concerning these data can be obtained from the lead contact, Yunjong Lee (ylee69@skku.edu) upon request. Detailed data points and statistical analyses for the quantification graphs in this study are provided in the supplemental information.
- Code: The article does not report the original code.
- Additional information: Any additional information for reanalysis of the presented results in this article will be available upon request from the lead contact, Yunjong Lee (ylee69@skku.edu).

ACKNOWLEDGMENTS

This research was supported by a grant of the Korea Dementia Research Project through the Korea Dementia Research Center (KDRC), funded by the Ministry of Health & Welfare and Ministry of Science and ICT, Republic of Korea (grant number:RS-2022-KH127042). And this work was also supported by the National Research Foundation of Korea (NRF) grant funded by the Korean government (MSIT) (RS-2024-00349023).

AUTHOR CONTRIBUTIONS

Y.L. and S-M.P. conceived the study hypothesis and supervised the project. J-Y.S. conducted the majority of the experiments and data analyses. M.W.H and S-M.P. designed and synthesized the molecules. J.H.K. and J.C. performed specific experiments (recombinant protein production, cortical neuron cultures) and data analyses. G.H.L. provided technical and material support. Y.L., S-M.P., and J-Y.S. wrote the article. All authors contributed to the final review of the article and figures.

DECLARATION OF INTERESTS

Y.L., J-Y.S., and S-M.P. are inventors listed on the domestic patent of the Republic of Korea (patent application no. 10-2022-0116705; title: "Inhibitors of abnormal protein aggregates and uses thereof"). The remaining authors declare no competing interests.

STAR★METHODS

Detailed methods are provided in the online version of this paper and include the following:

- KEY RESOURCES TABLE
- EXPERIMENTAL MODEL AND STUDY PARTICIPANT DETAILS
- METHOD DETAILS
  - Chemicals and antibodies
  - Synthesis of steroid derivatives
  - *In vitro* protein aggregation and Thioflavin T assay
  - Cell culture and trypan blue exclusion cell viability assessment
  - Real-time quantitative PCR
  - Dot blot assay
  - Primary cortical neuron culture and α-synuclein preformed fibril treatment
  - Immunofluorescence
  - Quantification of fluorescence images
  - Behavior tests
  - Immunohistochemistry
  - H&E staining of organ sections
- QUANTIFICATION AND STATISTICAL ANALYSIS

SUPPLEMENTAL INFORMATION

Supplemental information can be found online at https://doi.org/10.1016/j.isci.2024.111165.

Received: June 4, 2024
Revised: August 27, 2024
Accepted: October 9, 2024
Published: October 11, 2024

REFERENCES

1. Kalia, L.V., and Lang, A.E. (2015). Parkinson's disease. Lancet *386*, 896–912. https://doi.org/10.1016/S0140-6736(14)61393-3.
2. Forloni, G. (2023). Alpha Synuclein: Neurodegeneration and Inflammation. Int. J. Mol. Sci. *24*, 5914. https://doi.org/10.3390/ijms24065914.
3. Brahmachari, S., Ge, P., Lee, S.H., Kim, D., Karuppagounder, S.S., Kumar, M., Mao, X., Shin, J.H., Lee, Y., Pletnikova, O., et al. (2016). Activation of tyrosine kinase c-Abl contributes to alpha-synuclein-induced neurodegeneration. J. Clin. Invest. *126*, 2970–2988. https://doi.org/10.1172/JCI85456.
4. Flagmeier, P., Meisl, G., Vendruscolo, M., Knowles, T.P.J., Dobson, C.M., Buell, A.K., and Galvagnion, C. (2016). Mutations associated with familial Parkinson's disease alter the initiation and amplification steps of alpha-synuclein aggregation. Proc. Natl. Acad. Sci. USA *113*, 10328–10333. https://doi.org/10.1073/pnas.1604645113.
5. Ham, S., Yun, S.P., Kim, H., Kim, D., Seo, B.A., Kim, H., Shin, J.Y., Dar, M.A., Lee, G.H., Lee, Y.I., et al. (2020). Amyloid-like oligomerization of AIMP2 contributes to alpha-synuclein interaction and Lewy-like inclusion. Sci. Transl. Med. *12*, eaax0091. https://doi.org/10.1126/scitranslmed.aax0091.

6. Kam, T.I., Mao, X., Park, H., Chou, S.C., Karuppagounder, S.S., Umanah, G.E., Yun, S.P., Brahmachari, S., Panicker, N., Chen, R., et al. (2018). Poly(ADP-ribose) drives pathologic alpha-synuclein neurodegeneration in Parkinson's disease. Science *362*, eaat8407. https://doi.org/10.1126/science.aat8407.
7. Ross, O.A., Braithwaite, A.T., Skipper, L.M., Kachergus, J., Hulihan, M.M., Middleton, F.A., Nishioka, K., Fuchs, J., Gasser, T., Maraganore, D.M., et al. (2008). Genomic investigation of alpha-synuclein multiplication and parkinsonism. Ann. Neurol. *63*, 743–750. https://doi.org/10.1002/ana.21380.
8. Kim, H.Y., Kim, H.V., Jo, S., Lee, C.J., Choi, S.Y., Kim, D.J., and Kim, Y. (2015). EPPS rescues hippocampus-dependent cognitive deficits in APP/PS1 mice by disaggregation of amyloid-beta oligomers and plaques. Nat. Commun. *6*, 8997. https://doi.org/10.1038/ncomms9997.
9. Shin, J.Y., Lee, B., Ham, S., Kim, J.H., Kim, H., Kim, H., Jo, M.G., Kim, H.J., Park, S.W., Kweon, H.S., et al. (2022). Pharmacological inhibition of AIMP2 aggregation attenuates alpha-synuclein aggregation and toxicity in Parkinson's disease. Biomed. Pharmacother. *156*, 113908. https://doi.org/10.1016/j.biopha.2022.113908.
10. Zhang, W., Liu, W., Zhao, Y.D., Xing, L.Z., Xu, J., Li, R.J., and Zhang, Y.X. (2024). The potential of Rhein's aromatic amines for Parkinson's disease prevention and treatment: alpha-Synuclein aggregation inhibition and disaggregation of preformed fibers. Bioorg. Med. Chem. Lett. *97*, 129564. https://doi.org/10.1016/j.bmcl.2023.129564.
11. Hirohata, M., Ono, K., Morinaga, A., Ikeda, T., and Yamada, M. (2009). Anti-aggregation and fibril-destabilizing effects of sex hormones on alpha-synuclein fibrils *in vitro*. Exp. Neurol. *217*, 434–439. https://doi.org/10.1016/j.expneurol.2009.03.003.
12. Ko, H.S., von Coelln, R., Sriram, S.R., Kim, S.W., Chung, K.K.K., Pletnikova, O., Troncoso, J., Johnson, B., Saffary, R., Goh, E.L., et al. (2005). Accumulation of the authentic parkin substrate aminoacyl-tRNA synthetase cofactor, p38/JTV-1, leads to catecholaminergic cell death. J. Neurosci. *25*, 7968–7978. https://doi.org/10.1523/JNEUROSCI.2172-05.2005.
13. Carroll, J.S., and Brown, M. (2006). Estrogen receptor target gene: an evolving concept. Mol. Endocrinol. *20*, 1707–1714. https://doi.org/10.1210/me.2005-0334.
14. do Carmo, C.A., Gonçalves, Á.L.M., Salvadori, D.M.F., and Maistro, E.L. (2012). Nandrolone androgenic hormone presents genotoxic effects in different cells of mice. J. Appl. Toxicol. *32*, 810–814. https://doi.org/10.1002/jat.1701.
15. Kim, H., Maeng, H.J., Kim, J.H., Yoon, J.H., Oh, Y., Paek, S.M., and Lee, Y. (2022). Synthetic Peucedanocoumarin IV Prevents alpha-Synuclein Neurotoxicity in an Animal Model of Parkinson's Disease. Int. J. Mol. Sci. *23*, 8618. https://doi.org/10.3390/ijms23158618.
16. Estaun-Panzano, J., Arotcarena, M.L., and Bezard, E. (2023). Monitoring alpha-synuclein aggregation. Neurobiol. Dis. *176*, 105966. https://doi.org/10.1016/j.nbd.2022.105966.
17. Pujols, J., Peña-Díaz, S., Lázaro, D.F., Peccati, F., Pinheiro, F., González, D., Carija, A., Navarro, S., Conde-Giménez, M., García, J., et al. (2018). Small molecule inhibits alpha-synuclein aggregation, disrupts amyloid fibrils, and prevents degeneration of dopaminergic neurons. Proc. Natl. Acad. Sci. USA *115*, 10481–10486. https://doi.org/10.1073/pnas.1804198115.
18. Leidenheimer, N.J., and Ryder, K.G. (2014). Pharmacological chaperoning: a primer on mechanism and pharmacology. Pharmacol. Res. *83*, 10–19. https://doi.org/10.1016/j.phrs.2014.01.005.
19. Bernal, A., and Paolieri, D. (2022). The influence of estradiol and progesterone on neurocognition during three phases of the menstrual cycle: Modulating factors. Behav. Brain Res. *417*, 113593. https://doi.org/10.1016/j.bbr.2021.113593.
20. Dluzen, D.E., McDermott, J.L., and Liu, B. (1996). Estrogen as a neuroprotectant against MPTP-induced neurotoxicity in C57/B1 mice. Neurotoxicol. Teratol. *18*, 603–606. https://doi.org/10.1016/0892-0362(96)00086-4.
21. Ramirez, A.D., Liu, X., and Menniti, F.S. (2003). Repeated estradiol treatment prevents MPTP-induced dopamine depletion in male mice. Neuroendocrinology *77*, 223–231. https://doi.org/10.1159/000070277.
22. Brann, D.W., Dhandapani, K., Wakade, C., Mahesh, V.B., and Khan, M.M. (2007). Neurotrophic and neuroprotective actions of estrogen: basic mechanisms and clinical implications. Steroids *72*, 381–405. https://doi.org/10.1016/j.steroids.2007.02.003.
23. Coe, J.E., Ishak, K.G., and Ross, M.J. (1998). Estrogen-induced hepatic toxicity and hepatic cancer: differences between two closely related hamster species. Liver *18*, 343–351. https://doi.org/10.1111/j.1600-0676.1998.tb00816.x.
24. Rubinow, K.B. (2017). Estrogens and Body Weight Regulation in Men. Adv. Exp. Med. Biol. *1043*, 285–313. https://doi.org/10.1007/978-3-319-70178-3_14.
25. Travis, R.C., and Key, T.J. (2003). Oestrogen exposure and breast cancer risk. Breast Cancer Res. *5*, 239–247. https://doi.org/10.1186/bcr628.
26. Bjorklund, A., Nilsson, F., Mattsson, B., Hoban, D.B., and Parmar, M. (2022). A Combined alpha-Synuclein/Fibril (SynFib) Model of Parkinson-Like Synucleinopathy Targeting the Nigrostriatal Dopamine System. J. Parkinsons Dis. *12*, 2307–2320. https://doi.org/10.3233/JPD-223452.

STAR★METHODS

KEY RESOURCES TABLE

REAGENT or RESOURCE	SOURCE	IDENTIFIER
Antibodies		
Mouse anti-MAP2	Sigma-Aldrich	Cat# M4403; RRID: AB_477193
Mouse anti-pS129-αSyn	BioLegend	Cat# 825701: RRID: AB_2564891
Rabbit anti-pS129-αSyn	Abcam	Cat# ab51253: RRID: AB_869973
Rabbit anti-AIMP2	Proteintech	Cat# 10424-1-AP; RRID: AB_513880
Rabbit anti-eGFP	Cell Signaling Technology	Cat# 2956; RRID: AB_1196615
Mouse anti-α-synuclein	BD	Cat# 610787; RRID: AB_398108
Mouse anti- tyrosine hydroxylase	Immuno Star	Cat# 22941; RRID: AB_572268
Rabbit anti- tyrosine hydroxylase	Novus Biologicals	Cat# NB300-109; RRID: AB_10077691
Mouse anti-GFAP	Abcam	Cat# ab7260; RRID: AB_305808
biotin-conjugated goat antibody to rabbit IgG	Vector Laboratories	Cat# BA-1000; RRID: AB_2313606
biotin-conjugated goat antibody to mouse IgG	Vector Laboratories	Cat# BA-9200; RRID: AB_2336171
Alexa Fluor 568 donkey anti-rabbit IgG	Thermo Fisher Scientific	Cat# A10042; RRID: AB_2534017
Alexa Fluor 568 donkey anti-mouse IgG	Thermo Fisher Scientific	Cat# A10037; RRID: AB_11180865
Alexa Fluor 488 donkey anti-rabbit IgG	Thermo Fisher Scientific	Cat# A11008; RRID: AB_143165
Alexa Fluor 488 donkey anti-mouse IgG	Thermo Fisher Scientific	Cat# A21202; RRID: AB_141607
Alexa Fluor 405 goat anti-rabbit IgG	Thermo Fisher Scientific	Cat# A31556; RRID: AB_221605
Bacterial and virus strains		
AAV-eGFP	Vector Builder	N/A
AAV-αSyn	Vector Builder	N/A
Chemicals, peptides, and recombinant proteins		
Estriol	Sigma-Aldrich	Cat# E1253
Estrone 3-methyl ether	Tokyo Chemical Industry	Cat# E0917
3-methoxy-17-methylestra-1(10),2,4-trien-17-ol	Gregory L. Lackner et al.	https://doi.org/10.1021/ja408971t
Estrone	Tokyo Chemical Industry	Cat# E0026
Estradiol 3-methyl ether	Sen Yang et al.	https://doi.org/10.1021/acscatal.3c04075
Nandrolone	Tokyo Chemical Industry	Cat# N0777
SG13-135	This paper	N/A
SG13-136	This paper	N/A
SG13-138	This paper	N/A
SG13-140	This paper	N/A
SG13-141	This paper	N/A
SG13-158	This paper	N/A
Sodium hydride	Sigma-Aldrich	Cat# 452912
1-bromo-2-methylpropane	Sigma-Aldrich	Cat# 156582
Lithium aluminum hydride	Sigma-Aldrich	Cat# 199877
N-(3-Azidopropyl) biotinamide	Sigma-Aldrich	Cat# 935395
Thioflavin T	Sigma-Aldrich	Cat# T3516-25G
Trypan blue	Sigma-Aldrich	Cat# T8154-20ML
Dulbecco's modified Eagle's medium (DMEM)	Gibco	Cat# 11995073
Fetal bovine serum (FBS)	Gibco	Cat# 26140079
penicillin–streptomycin antibiotic solution	Sigma-Aldrich	Cat# 4333

(*Continued on next page*)

Continued

REAGENT or RESOURCE	SOURCE	IDENTIFIER
X-tremeGENE HP DNA Transfection Reagent	Roche	Cat# 6366546001
QIAzol Lysis solution	QIAGEN	Cat# 79306
SYBR-Green PCR mixture	Applied Biosystems	Cat# 4309155
Minimum Essential Medium (MEM)	Gibco	Cat# 11090081
5% normal goat serum	Invitrogen	Cat# 16201
0.1% Triton X-100	Sigma-Aldrich	Cat# X100
DAPI	Sigma-Aldrich	Cat# D9542
Immu-Mount	Thermo Fisher	Cat# 9990402
ABC-HRP solution	Vector Laboratories	Cat# PK-4000
3,3-diaminobenzidine	Sigma-Aldrich	Cat# D4293
4% Paraformaldehyde Solution	Biosesang	Cat# PC2031-100-00
Hematoxylin	Merck	Cat# 318906
Eosin	Merck	Cat# MHS32
Heparin	Sigma-Aldrich	Cat# H3393
GST recombinant protein	Ham et al.[5]	N/A
Tau recombinant protein	Abcam	Cat# ab199583
PARIS recombinant protein	Laboratory production	N/A
AIMP2 recombinant protein	Ham et al.[5]	N/A
αSyn recombinant protein	Ham et al.[5]	N/A
Critical commercial assays		
cDNA Synthesis kit	Bio-Rad	Cat# 170-8891
Experimental models: Cell lines		
Human neuroblastoma SH-SY5Y cells	ATCC	Cat# CRL-2266
Human MCF7 cells	ATCC	Cat# HTB-22
Mouse cortical neurons	N/A	N/A
Experimental models: Organisms/strains		
Mouse: CrlOri:CD1(ICR) mice	Orient Bio animal company	N/A
Mouse: C57BL/6N mice	Orient Bio animal company	N/A
Oligonucleotides		
Primer: *Ebag9* (mouse) F: TGCCCACTACAGTTGATTATTCG R: AGTCAGGTTCCAGTTGTTCCA	Primer Bank	https://pga.mgh.harvard.edu/primerbank/
Primer: *Ccnd1* (mouse) F: GCGTACCCTGACACCAATCTC R: ACTTGAAGTAAGATACGGAGGGC	Primer Bank	https://pga.mgh.harvard.edu/primerbank/
Primer: *Gapdh* (mouse) F: AGGTCGGTGTGAACGGATTTG R: GGGGTCGTTGATGGCAACA	Primer Bank	https://pga.mgh.harvard.edu/primerbank/
Primer: *EBAG9* (human) F: AGTTCCTAAGCAGACAGATGTTG R: CCCATTCCCTCCTTCGATCTTTA	Primer Bank	https://pga.mgh.harvard.edu/primerbank/
Primer: *CCND1* (human) F: GCTGCGAAGTGGAAACCATC R: CCTCCTTCTGCACACATTTGAA	Primer Bank	https://pga.mgh.harvard.edu/primerbank/

(*Continued on next page*)

Continued

REAGENT or RESOURCE	SOURCE	IDENTIFIER
Primer: *E2F1* (human) F: ACGCTATGAGACCTCACTGAA R: TCCTGGGTCAACCCCTCAAG	Primer Bank	https://pga.mgh.harvard.edu/primerbank/
Primer: *BCL2* (human) F: GGTGGGGTCATGTGTGTGG R: CGGTTCAGGTACTCAGTCATCC	Primer Bank	https://pga.mgh.harvard.edu/primerbank/
Primer: *GAPDH* (human) F: GGAGCGAGATCCCTCCAAAAT R: GGCTGTTGTCATACTTCTCATGG	Primer Bank	https://pga.mgh.harvard.edu/primerbank/
Recombinant DNA		
β-galactosidase	Dr. Ted dawson lab	N/A
Myc	Ham et al.[5]	N/A
Myc-AIMP2	Ham et al.[5]	N/A
Software and algorithms		
Fluorescence-reader (SYNERGY neo microplate reader)	Bio Tek	https://www.biotek-lab.com/liquidhandling
QuantStudio 6 flex Real-Time quantitative PCR System	Thermo Fisher	https://www.thermofisher.com/order/catalog/product/4485691
ImageJ software v1.52a	NIH	https://imagej.nih.gov/ij/
GraphPad Prism v8	GraphPad Software Inc.	https://www.graphpad.com/updates
Optical Fractionator probe in Stereo Investigator software	Micro Brightfield	https://www.mbfbioscience.com/products/stereo-investigator
Other		
Dot blot machine (BIO-Dot)	BIO-RAD	Cat# 1706542
Cell strainer	Falcon	Cat# 352340
Countess II Automated Cell Counter	Life Technologies	Cat# AMQAX 1000
Fluorescence microscope	Carl Zeiss	Axiovert 200 M

EXPERIMENTAL MODEL AND STUDY PARTICIPANT DETAILS

Approval for drug administration animal experiments were obtained from the Institutional Animal Care and Use Committee of Sungkyunkwan University (SKKUIACUC2022-03-39-1). Male C57BL/6N mice (2 months old) were purchased from Orient Bio animal company (Seongnam, Korea). AAV-eGFP or AAV-αSyn was injected into the substantia nigra pars compacta (SNpc) (Coordinates from bregma, L: 1.3, AP: −3.4, DV: −4.3 mm), and PBS or αSyn PFF was injected into the ventral tegmental area (Coordinates from bregma, L: 0.5, AP: −3.4, DV: −4.3) of 2-months-old C57BL/6N mice.[5,26] To evaluate the effect of SG13-136, it was administered orally at a dose of 0.5 mg/kg once daily for 3 weeks. Only male mice of the same age were used in this study to minimize experimental variability within groups. Male and female mice may exhibit differential adverse effects in response to systemic administration of estriol, which was used as a reference compound for the potential toxicity of the estriol derivative SG13-136.

SH-SY5Y human neuroblastoma cells (ATCC, Manassas, VA; Female origin) were grown in Dulbecco's Modified Eagle Medium (DMEM) (Gibco, cat#11995073) supplemented with 10% fetal bovine serum (v/v, Gibco, cat#26140079) and 1% penicillin-streptomycin (100 U/ml, Sigma-Aldrich, cat#4333). The cells were maintained in a 37°C incubator under a humidified atmosphere containing 5% CO_2. This cell line was used to model AIMP2 toxicity via transient transfection of Myc-AIMP2 and evaluate therapeutic effects of steroid derivatives.

MCF7 human breast cancer cells (ATCC, Manassas, VA; Female origin) were cultured in Dulbecco's Modified Eagle Medium (DMEM) (Gibco, cat#11995073) supplemented with 10% fetal bovine serum (FBS) (v/v, Gibco, cat#26140079), and 1% penicillin-streptomycin (100 U/ml, Sigma-Aldrich, cat#4333). The cells were maintained in a humidified incubator at 37°C with 5% CO2. This cell line was used to determine estrogenic functions of steroid derivatives.

For mouse cortical neuron culture, fetal tissues (from both male and female embryos, though not identified in this study) was collected from ICR mice at gestational day 15, obtained from Orient Bio (Seongnam, Korea). Cortical tissue was dissected from the fetal brains, incubated in 0.05% trypsin-EDTA for 20 minutes at 37°C, then washed with 1× MEM and filtered through a 40 μm cell strainer (Falcon, cat#352340) after trypsinization. The cortical neuron suspension was plated on poly-L-lysine-coated 12-well plates and maintained by changing the medium (Neurobasal A medium (Gibco, cat#10888022) supplemented with B-27 (Gibco, cat#17504044) and 1 mM L-glutamine (Gibco,

cat#25030081)) every 3–4 days. After 7 days of cortical neuron differentiation, αSyn PFF (1 μg/ml, 10 days) was administered to model α-synucleinopathy.

METHOD DETAILS

Chemicals and antibodies

Thioflavin T (cat# T3516-25G) and trypan blue (cat# T8154-20ML) were procured from Sigma-Aldrich (St. Louis, Missouri, USA).

The primary antibodies used included: mouse antibody to MAP2 (Sigma-Aldrich, cat#M4403), mouse antibody to pS129-αSyn (BioLegend, cat#825701), rabbit antibody to pS129-αSyn (Abcam, cat# ab51253), rabbit antibody to AIMP2 (Proteintech, cat#10424-1-AP), mouse antibody to tyrosine hydroxylase (Immuno Star, cat#22941), and mouse antibody to GFAP (Abcam, cat#ab7260). Furthermore, the secondary antibodies used were: biotin-conjugated goat antibody to rabbit IgG (Vector Laboratories, cat#BA-1000), biotin-conjugated goat antibody to mouse IgG (Vector Laboratories, cat#BA-9200), Alexa Fluor 568 donkey anti-rabbit IgG (Invitrogen, cat#A10042), and Alexa Fluor 488 donkey anti-mouse IgG (Invitrogen, cat#A21202).

Estriol (cat# E1253-1G) was purchased from Sigma-Aldrich (St. Louis, Missouri, USA). Estrone (cat# E0026-), estrone 3-methyl ether (cat# E0917-) and nandrolone (cat# N0777-) were purchased from Tokyo Chemical Industry. Estradiol 3-methyl ether and 3-methoxy-17-methylestra-1(10),2,4-trien-17-ol were prepared by known procedures, respectively. Other compounds were synthesized as described below (synthesis of steroid derivatives).

Tetrahydrofuran was distilled from sodium benzophenone ketyl, and dichloromethane was freshly distilled from calcium hydride. All solvents used for routine isolation of products and chromatography were reagent grade. Moreover, air and moisture sensitive reactions were performed under an argon atmosphere. Flash column chromatography was performed using silica gel 60 (230–400 mesh, Merck, Darmstadt, Germany) with the indicated solvents, and thin-layer chromatography was performed using 0.25 mm silica gel plates (Merck). ^{1}H-NMR data were reported in the order of chemical shift, multiplicity (s: singlet; d: doublet; t: triplet; q: quartet; and m: multiplet and/or multiple resonance), number of protons, and coupling constant in hertz (Hz).

Synthesis of steroid derivatives

SG13-135; (8*R*,9*S*,13*S*,14*S*)-3-isobutoxy-13-methyl-6,7,8,9,11,12,13,14,15,16-decahydro-17*H*-cyclopenta[*a*]phenanthren-17-one.

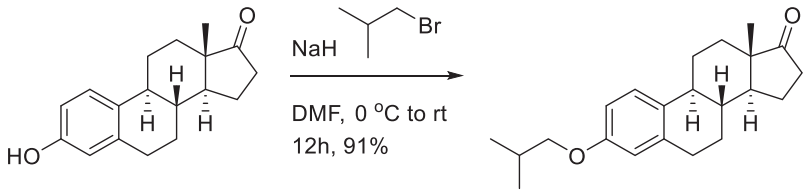

To a solution of estrone (1.0 g, 3.7 mmol) in DMF (10 mL), sodium hydride (60% in mineral oil, 178 mg, 4.4 mmol) was added at 0°C. After 30 min, 1-bromo-2-methylpropane (0.48 mL, 4.4 mmol) was added to reaction mixture. After stirring the reaction mixture at room temperature for 12 h, aq. NH_4Cl was treated for quenching. Reaction mixture was diluted with EtOAc and extracted with H_2O three times. Organic layers were dried over $MgSO_4$, filtered and concentrated. The residue was purified on silica-gel chromatography (EtOAc:n-hexane = 1:5) to provide 1.1 g (91%) of **SG13-135** as a white solid.

$[\alpha]_D^{25}$ = 112.86° (*c* = 1.0, $CHCl_3$); ^{1}H-NMR ($CDCl_3$, 500 MHz) δ 7.17 (1H, d, *J* = 8.5 HZ), 6.70 (1H, dd, *J* = 8.5, 2.5 Hz), 6.62 (1H, d, *J* = 2.5 Hz), 3.67 (2H, d, *J* = 7.0 Hz), 2.88 (2H, m), 2.48 (1H, dd, *J* = 19.0, 8.5 Hz), 2.37 (1H, m), 2.32 (1H, m), 2.14-1.92 (5H, m), 1.60-1.39 (6H, m), 1.00 (3H, s), 0.98 (3H, s), 0.89 (3H, s); ^{13}C-NMR ($CDCl_3$, 125 MHz) δ 157.3, 137.6, 131.7, 126.2, 114.5, 112.1, 74.4, 50.4, 67.0, 66.0, 38.4, 35.8, 31.6, 29.6, 28.3, 26.5, 25.9, 21.6, 19.2(2C), 13.8. FT-IR (ATR) ν_{max} 2929, 1737, 1498, 1231, 1036, 1005, 816 cm^{-1}. HRMS (TOF): Calcd. for $C_{22}H_{31}O_2$ ($[M+H]^+$): 327.2324, found: 327.2317.

SG13-136; (8*R*,9*S*,13*S*,14*S*,17*R*)-3-isobutoxy-13-methyl-7,8,9,11,12,13,14,15,16,17-decahydro-6*H*-cyclopenta[*a*]phenanthren-17-ol.

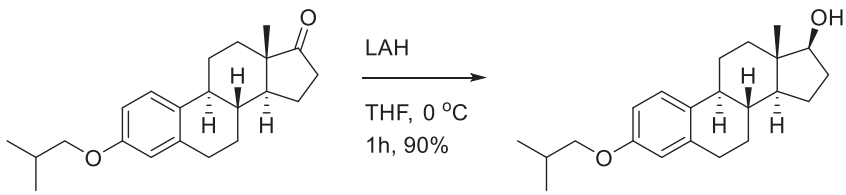

To a solution of **SG13-135** (210 mg, 0.64 mmol) in THF (10 mL), lithium aluminum hydride (24 mg, 0.64 mmol) was added at 0°C. After stirring the reaction mixture for 1 h, H_2O was added slowly at 0°C. After filter the solid mixture, organic residue was dried over $MgSO_4$, filtered and concentrated. The residue was purified on silica-gel chromatography (EtOAc:n-hexane = 1:2) to provide 190 mg (90%) of **SG13-136** as a white solid.

$[\alpha]_D^{25}$ = 44.54° (*c* = 1.0, $CHCl_3$); ^{1}H-NMR ($CDCl_3$, 500 MHz) δ 7.18 (1H, d, *J* = 8.5 HZ), 6.70 (1H, dd, *J* = 8.5, 2.5 Hz), 6.62 (1H, d, *J* = 2.5 Hz), 3.71 (1H, t, *J* = 8.5 Hz), 3.67 (2H, d, *J* = 7.0 Hz), 2.84 (2H, m), 2.30 (1H, m), 2.17 (1H, m), 2.15-2.03 (2H, m), 1.94 (1H, dt, *J* = 12.5, 3.5 Hz), 1.86 (1H, m), 1.68 (1H, m), 1.50-1.11 (7H, m), 1.00 (3H, s), 0.99 (3H, s), 0.77 (3H, s); ^{13}C-NMR ($CDCl_3$, 125 MHz) δ 157.2, 137.9, 132.4, 126.3, 114.5, 112.0, 81.8, 74.4, 50.1, 44.0, 43.3, 38.9, 36.8, 30.5, 29.8, 28.3, 27.3, 26.4, 23.2, 19.3, 11.1. FT-IR (ATR) ν_{max} 3328, 2954, 2912, 2866, 1611, 1499, 1470 cm^{-1}. HRMS (TOF): Calcd. for $C_{22}H_{33}O_2$ ($[M+H]^+$): 329.2481, found: 329.2480.

SG13-138; (8*R*,9*S*,13*S*,14*S*)-3-isobutoxy-13-methyl-6,7,8,9,11,12,13,14,15,16-decahydro-17*H*-cyclopenta[*a*]phenanthren-17-one oxime.

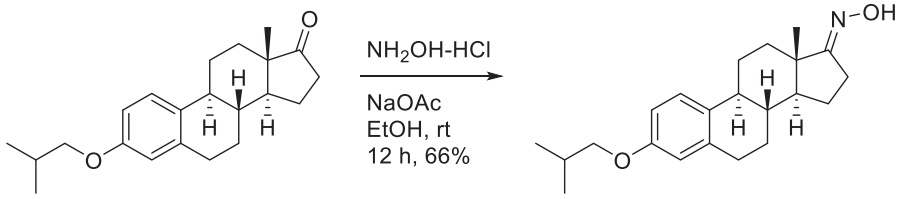

To a solution of **SG13-135** (74 mg, 0.23 mmol) in EtOH (4 mL), NH_2OH-HCl (19 mg, 0.27 mmol) and NaOAc (45 mg, 0.54 mmol) were added. After stirring the reaction mixture at room temperature for 12 h, aq. NH_4Cl was treated for quenching. Reaction mixture was diluted with H_2O and extracted with EtOAc twice. Organic layers were dried over $MgSO_4$, filtered and concentrated. The residue was purified on silica-gel chromatography (EtOAc:n-hexane = 1:2) to provide 52 mg (66%) of **SG13-138** as a yellow solid.

$[\alpha]_D^{25}$ = 46.68° (*c* = 1.0, $CHCl_3$); ^{1}H-NMR ($CDCl_3$, 500 MHz) δ 7.84 (1H, s), 7.17 (1H, d, *J* = 8.5 HZ), 6.69 (1H, dd, *J* = 8.5, 2.5 Hz), 6.61 (1H, d, *J* = 2.5 Hz), 3.67 (2H, d, *J* = 6.5 Hz), 2.88 (2H, m), 2.56 (2H, m), 2.35 (1H, dd, *J* = 13.5, 3.0 Hz), 2.25 (1H, m), 2.05-2.00 (2H, m), 1.95-1.90 (2H, m), 1.60-1.39 (6H, m), 0.99 (3H, s), 0.98 (3H, s), 0.86 (3H, s); ^{13}C-NMR ($CDCl_3$, 100 MHz) δ 157.3, 137.6, 131.7, 126.2, 114.5, 112.1, 74.4, 53.0, 44.8, 43.8, 38.1, 33.8, 29.6, 28.3, 27.2, 26.1, 22.8, 19.2 (2C), 17.0. FT-IR (ATR) ν_{max} 3261, 2959, 2916, 2877, 1606, 1499 cm^{-1}. HRMS (TOF): Calcd. for $C_{22}H_{31}NO_2^+$ ($[M]^+$): 341.2355, found: 341.2355.

SG13-140; (8*R*,9*S*,13*S*,14*S*,17*R*)-3-isobutoxy-13,17-dimethyl-7,8,9,11,12,13,14,15,16,17-decahydro-6*H*-cyclopenta[*a*]phenanthren-17-ol.

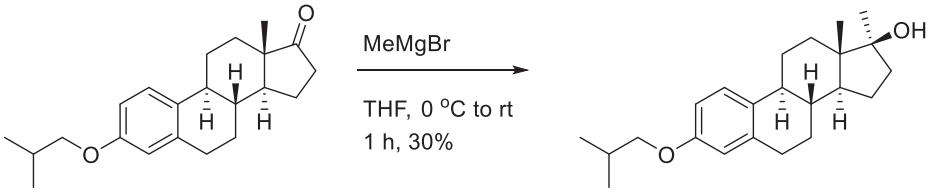

To a solution of **SG13-135** (530 mg, 1.6 mmol) in THF (10 mL), MeMgBr (3.0M in Et_2O, 0.8 mL, 2.4 mmol) was added 3 times at 0°C. After stirring the reaction mixture at room temperature for 1 h, aq. NH_4Cl was treated for quenching. Reaction mixture was diluted with H_2O and extracted with EtOAc twice. Organic layers were dried over $MgSO_4$, filtered and concentrated. The residue was purified on silica-gel chromatography (EtOAc:n-hexane = 1:5 to 1:2) to provide 170 mg (30%) of **SG13-140** as a white solid.

$[\alpha]_D^{25}$ = 65.73° (*c* = 1.0, $CHCl_3$); ^{1}H-NMR ($CDCl_3$, 500 MHz) δ 7.17 (1H, d, *J* = 8.5 HZ), 6.70 (1H, dd, *J* = 8.5, 2.5 Hz), 6.62 (1H, d, *J* = 2.0 Hz), 3.68 (2H, d, *J* = 7.0 Hz), 2.89-2.80 (2H, m), 2.31 (1H, m), 2.15 (1H, m), 2.04 (1H, m), 1.87 (1H, m), 1.79 (2H, m), 1.51-1.30 (8H, m) 1.26 (3H, s), 1.00 (3H, s), 0.98 (3H, s), 0.89 (3H, s); ^{13}C-NMR ($CDCl_3$, 100 MHz) δ 157.1, 137.9, 132.4, 126.2, 114.5, 112.0, 81.7, 74.4, 49.7, 45.8, 39.7, 39.0, 31.7, 29.8, 28.3, 27.5, 26.3, 25.8, 22.9, 19.3 (2C), 13.9. FT-IR (ATR) ν_{max} 3335, 2931, 2869, 1611, 1497, 1234 cm^{-1}. HRMS (TOF): Calcd. for $C_{23}H_{34}O_2^+$ ($[M]^+$): 342.2559, found: 342.2560.

SG13-141; (8*R*,9*S*,13*S*,14*S*,17*R*)-3-isobutoxy-13-methyl-7,8,9,11,12,13,14,15,16,17-decahydro-6*H*-cyclopenta[*a*]phenanthren-17-yl propionate.

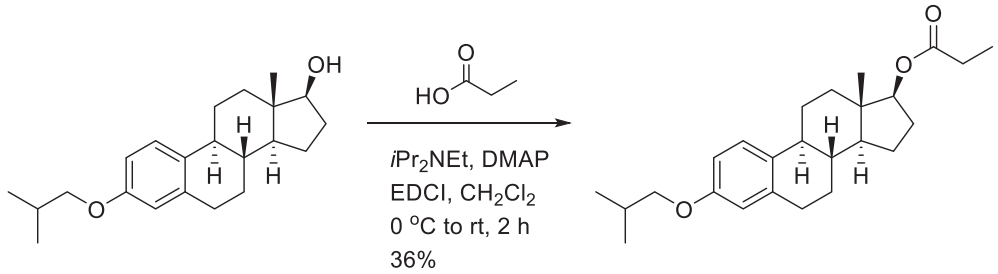

To a solution of **SG13-136** (500 mg, 1.5 mmol) in CH_2Cl_2 (10 mL), *i*Pr_2NEt (0.52 mL, 3.0 mmol), DMAP (36 mg, 0.3 mmol), EDCI (580 mg, 3.0 mmol) and propionic acid (0.23 mL, 3.0 mmol) were added at 0°C. After stirring the reaction mixture at room temperature for 12 h, aq. NH_4Cl was treated for quenching. Reaction mixture was diluted with H_2O and extracted with CH_2Cl_2 twice. Organic layers were dried over $MgSO_4$, filtered and concentrated. The residue was purified on silica-gel chromatography (EtOAc:n-hexane = 1:10 to 1:5) to provide 210 mg (36%) of **SG13-141** as a colorless liquid.

$[\alpha]_D^{25}$ = 35.91° (*c* = 1.0, $CHCl_3$); ^{1}H-NMR ($CDCl_3$, 400 MHz) δ 7.20 (1H, d, *J* = 8.8 HZ), 6.72 (1H, dd, *J* = 8.8, 2.4 Hz), 6.66 (1H, d, *J* = 2.4 Hz), 4.74 (1H, t, *J* = 8.0 Hz), 3.71 (2H, d, *J* = 6.8 Hz), 2.87 (2H, m), 2.37 (2H, q, *J* = 7.6 Hz). 2.35 – 2.15 (3H, m), 2.07 (1H, m), 1.91 (2H, m), 1.77 (2H, m), 1.59 – 1.25 (6H, m), 1.19 (3H, t, *J* = 9.2 Hz), 1.06 (3H, s), 1.04 (3H, s), 0.86 (3H, s); ^{13}C-NMR ($CDCl_3$, 100 MHz) δ 174.4, 157.2, 137.7, 132.2, 125.3, 114.5, 112.0, 82.5, 74.3, 49.8, 43.8, 43.0, 38.6, 37.0, 29.8, 28.3, 27.8, 27.7, 27.3, 26.3, 23.3, 19.3, 12.1, 9.3. FT-IR (ATR) ν_{max} 2967, 2916, 2869, 1730, 1609, 1278 cm^{-1}. HRMS (TOF): Calcd. for $C_{25}H_{37}O_3$, ($[M+H]^+$): 385.2743, found 385.2747:.

SG13-158; *N*-(3-(4-((((8*R*,9*S*,13*S*,14*S*,17*S*)-17-hydroxy-13-methyl-7,8,9,11,12,13,14,15,16,17-decahydro-6*H*-cyclopenta[*a*]phenanthren-3-yl)oxy)methyl)-1H-1,2,3-triazol-1-yl)propyl)-5-((3a*S*,4*S*,6a*R*)-2-oxohexahydro-1*H*-thieno[3,4-*d*]imidazol-4-yl)pentanamide.

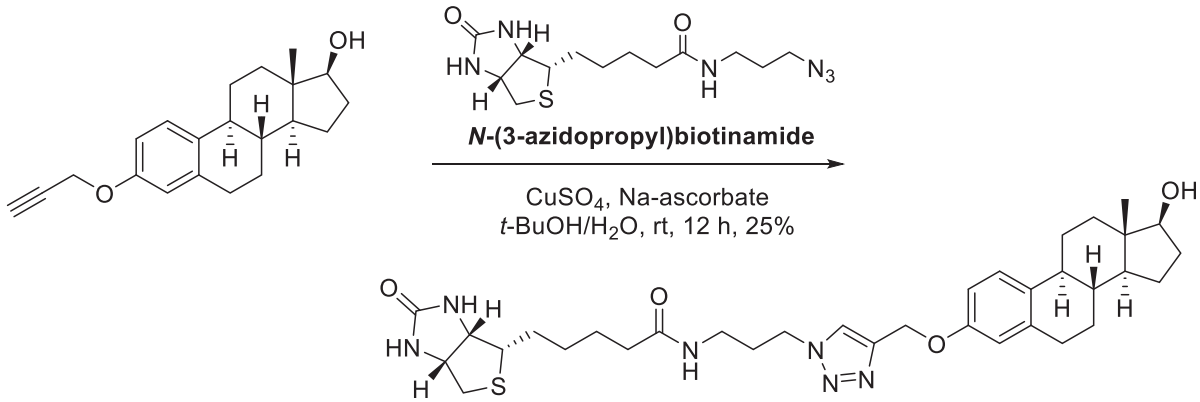

To a solution of the propargyl estradiol (140 mg, 0.44 mmol) in *t*-BuOH/H_2O (4mL/4mL), *N*-(3-azidopropyl)biotinamide (170 mg, 0.53 mmol), $CuSO_4$ (7 mg, 0.044 mmol) and sodium ascorbate (17 mg, 0.088mmol) were added. After stirring the reaction mixture at room temperature for 24 h, reaction mixture evaporated and purified on silica-gel chromatography (CH_2Cl_2:MeOH = 15:1) to provide 72 mg (25%) of **SG13-158** as a yellow solid.

$[\alpha]_D^{25}$ = 35.97° (*c* = 1.0, CH_3OH); ^{1}H-NMR (CD_3OD, 500 MHz) δ 7.93 (1H, s), 7.07 (1H, d, *J* = 8.5 HZ), 6.64 (1H, dd, *J* = 8.5, 2.5 Hz), 6.58 (1H, d, *J* = 2.5 Hz), 4.99 (2H, s), 4.36 (1H, m), 4.33 (2H, t, *J* = 7.0 Hz), 4.17 (1H, m), 3.54 (1H, t, *J* = 9.0 Hz), 3.14-3.06 (3H, m), 2.79 (2H, dd, *J* = 13,0, 5.0 Hz), 2.71 (2H, m), 2.58 (1H, d, *J* = 13.0 Hz), 2.21 (1H, m), 2.09 (2H, t, *J* = 7.5 Hz), 2.05 (1H, m), 2.00 (2H, *J* = 7.5 Hz), 1.95 – 1.83 (2H, m), 1.75 (1H, m), 1.68 – 1.00 (16H, m), 0.66 (3H, s); ^{13}C-NMR (CD_3OD, 125 MHz) δ 174.8, 164.6, 156.1, 143.9, 137.7, 133.1, 126.0, 124.0, 114.4, 112.0, 81.0, 61.9, 60.9, 60.2, 55.6, 49.9, 48.7, 43.9, 42.9, 39.6, 39.0, 36.6, 36.0, 35.3, 297, 29.4, 29.3, 28.4, 28.0, 27.0, 26.1, 25.3, 10.3. FT-IR (ATR) ν_{max} 3276, 2924, 2864, 1686, 1646, 1455 cm^{-1}. HRMS (TOF): Calcd. for $C_{34}H_{49}N_6O_4S$ ($[M+H]^+$): 637.3536, found: 637.3540.

In vitro protein aggregation and Thioflavin T assay

The combination of recombinant AIMP2 (1 μM), α-synuclein monomer (1 μM), or tau (20 μM with 5 μM heparin) and compound (50 μM) was incubated for 3 days at 37°C. The formation of AIMP2 aggregates was then assessed using thioflavin T fluorescence plate reading. Specifically, 0.8 μl of Thioflavin T solution at a concentration of 25 μM was mixed with 80 μl of proteins from each group. Subsequently, the mixture was allowed to incubate at 37°C for 15 minutes, and the fluorescence was measured using a fluorescence-reader (SYNERGY neo microplate reader, Bio Tek) with excitation conditions set at 450 nm and emission conditions at 480 nm.

Cell culture and trypan blue exclusion cell viability assessment

Human neuroblastoma SH-SY5Y cells (ATCC, Manassas, VA) were cultured in Dulbecco's modified Eagle's medium (DMEM) (Gibco, cat#11995073), supplemented with 10% fetal bovine serum (v/v, Gibco, cat#26140079), and 1% penicillin–streptomycin antibiotic solution (100 U/ml, Sigma-Aldrich, cat#4333). The culture was maintained in a humidified 5% CO_2 atmosphere at 37°C. For transient transfection, SH-SY5Y cells were transfected with Myc-AIMP2 plasmids using X-tremeGENE HP DNA Transfection Reagent at a 3:1 ratio (Roche, cat#6366546001). After 24 h, each compound (final concentration 10 μM) was added to DMEM, supplemented with 2.5% fetal bovine serum and dispensed. Cells were harvested 48 h later, involving trypsinization, two washes with 1× PBS, and re-suspension in 1× PBS. The re-suspended cells were mixed with an equal volume of 0.4% trypan blue (w/v) and incubated for 2 minutes at 25°C. Live and dead cells were counted using a Countess II Automated Cell Counter (Life Technologies, Bothell, WA, USA).

Real-time quantitative PCR

To prevent DNA contamination, RNA extraction was performed from MCF7 cells and mouse brain tissues using QIAzol Lysis solution (QIAGEN, cat#79306), followed by treatment with DNase I. For cDNA synthesis, 1 μg of RNA was used from a cDNA Synthesis kit (Bio-Rad, cat#170-8891). Real-time quantitative PCR was then conducted on the cDNA using SYBR-Green PCR mixture (Applied Biosystems, cat#4309155) and the QuantStudio 6 flex Real-Time quantitative PCR System. The comparative mRNA expression of target genes was calculated using the ΔΔCt method with GAPDH as a loading control. The primer information is provided in the key resources table.

Dot blot assay

Two sheets of 3M paper and one sheet of membrane are placed on the dot blot machine (BIO-Dot BIO-RAD, cat#1706542), and the screws were tightened. Samples, 100 μl each, were loaded through vacuum into each well. The vacuum was locked after sample loading, and the loaded samples was checked using Ponceau staining. Ponceau was removed with 1× TBS-T and blocking was done for 1 hour with 5% skim milk at RT. Subsequently, the membrane is washed, and the primary antibody is added, followed by incubation on a shaker for 1 hour at 4°C. After 1 hour, it was washed three times, and a mixture of 5% skim milk (10 ml) and secondary antibody (2 μl) in a ratio of 5000:1 was prepared. This solution was then applied to the membrane and incubated on a shaker at room temperature for 30 minutes. Following incubation, the membrane was washed with 1× TBS-T, and the development step was carried out in a dark room.

Primary cortical neuron culture and α-synuclein preformed fibril treatment

The day before culturing, the plate was coated with PLL along with glass, washed on the next day, and exposed to UV for 1 h. Fetuses were obtained from ICR mice (15 days after gestation) procured from Orient Bio animal company (Seongnam, Korea). Only cortex tissue was retrieved from the fetal brain. The cortex tissue was incubated in 1× trypsin EDTA (0.05%) for 20 minutes at 37°C, washed with 1× MEM, and then filtered through a cell strainer after trypsinization (Falcon cat#352340, 40 μm). The resulting neuron mixture was plated on a coated 12-well culture plate. The neurons were maintained by changing the medium every 3–4 days. After nine days, drug treatment and validation experiments were conducted. Additionally, to induce α-synucleinopathy in cultured neurons, sonicated αSyn PFF (final concentration of 1 μg/ml) were added to differentiated mouse cortical neurons and incubated for 10 days.

Immunofluorescence

Cells fixed with 4% paraformaldehyde were blocked for 1 h with a solution containing 5% normal goat serum (Invitrogen, cat#16201) and 0.1% Triton X-100 (Sigma-Aldrich, cat#X100). Subsequently, samples were incubated overnight at 4°C with combinations of primary antibodies against AIMP2, pS129-αSyn, and MAP2, depending on the experiment. Following overnight incubation, samples were washed with 1× PBS and then incubated with the corresponding secondary antibody conjugated with a fluorescent dye for 1 h at room temperature. After further washing with 1× PBS, samples were incubated with DAPI (Sigma-Aldrich, cat#D9542) for 1 min for nuclear staining. Subsequently, the samples were mounted using Immu-Mount (Thermo Fisher, cat#9990402). Fluorescence images were obtained using a fluorescence microscope (Axiovert 200 M, Zeiss, Oberkochen, Germany).

Quantification of fluorescence images

Signal quantification was obtained as mean fluorescence intensity per area using ImageJ software (National Institutes of Health, Bethesda, MD, USA). In detail, images in TIFF format were loaded in ImageJ, and regions of interest (ROIs) corresponding to specific regions were manually outlined using the freehand selection tool. With ROI selected, it was measured using Analysis > Measurement Tool. As a result, we obtained the integrated density and area of the selected ROI. The average fluorescence intensity was calculated by dividing the integrated density by the ROI area. Finally, statistical analysis was performed to compare fluorescence intensities between different experimental groups.

Behavior tests

Pole test

Prior to conducting the pole test, mice underwent two training sessions. The pole used in the test was a 23-inch-long metal rod wrapped with bandage gauze of 9-mm diameter. Mice were positioned facing head-down on the top of the pole, and the total latency to reach the ground was measured. Results were presented as the mean time taken to descend from the pole over three trials.

Rotarod test

Before conducting the rotarod test, mice underwent a 2-day training period. On the third day, mice were positioned on an accelerating rotarod cylinder, and the time until they dropped from the cylinder was recorded. The speed of the rotarod was gradually increased from 4 to 40 rpm over a 5-minute period while the mice were on the accelerating rotarod, and the duration until they fell off was measured. Each trail ended once the mouse fell off the rotarod. Data were presented as the mean latency to fall across three trials.

Body weights measurement

Throughout the 3-week experiment, the weight of each mouse was measured every two days using an electronic scale while the mouse remained immobile. After measurements were taken for up to 20 days, changes in weight were confirmed using the body weight graph.

Immunohistochemistry

The collected brain tissue was transferred to a plate containing a blocking solution using a brush and left on a rocker at room temperature for 30 minutes. Primary antibodies (TH, pS129-αSyn and GFAP) (1:1000), diluted in the blocking solution, were added to new plate wells, and after

30 minutes, the brain tissue was collected and transferred. It was then incubated overnight at 4°C on a rocker. Following overnight incubation, the brain was washed in PBS containing TritonX-100. After washing, it was placed in secondary antibodies and rocked at room temperature for 1 hour. Subsequently, after another washing process, the brain tissue was exposed to ABC solution (Vector Laboratories) and incubated for 40 minutes at room temperature. It was then treated with 3,3-diaminobenzidine (DAB, cat# D4293, Sigma), shaken, and stained. The stained brain tissue was mounted on a glass slide and allowed to dry. For TH stereological cell counting, the Optical Fractionator probe in Stereo Investigator software (MicroBrightfield, Williston, VT) was utilized to determine the total number of TH-positive neurons observed with DAB in the substantia nigra pars compacta.

H&E staining of organ sections

The tissues, fixed in 4% PFA and embedded in 30% sucrose, were sliced to a thickness of 40 μm for pathological evaluation, and the sections were placed on glass slides. Following dehydration, the sections were stained with hematoxylin (Merck, cat#318906) for 3 min and eosin (Merck, cat#MHS32) for 1 min. Subsequently, the sections were destained by rinsing in gradually increasing concentrations of a water/ethanol solution. After fixing in xylene, they were mounted using DPX mounting solution (Sigma-Aldrich, cat#06522). Images were captured using a microscope (Axiovert, 200M, Carl Zeiss, Germany).

QUANTIFICATION AND STATISTICAL ANALYSIS

Quantitative data are presented as mean ± SEM. Statistical significance was assessed using either an unpaired two tailed Student's *t*-test (comparisons of two group) or analysis of variance test with Turkey's HSD post hoc analysis (comparisons of more than three groups). Moreover, Graph Pad Prism software was utilized for preparing all plots and conducting statistical analyses. Differences with a *P*-value of < 0.05 were considered statistically significant. The statistical analysis and exact value of n used in each quantified graph are reported in the figure legends. Detailed statistical information and data points are presented in the Table S2.